DOI: 10.1002/chem.200600324

Structure and Bonding in First-Row Transition-Metal Dicarbides: Are They Related to the Stability of Met-cars?

Víctor M. Rayón, Pilar Redondo, Carmen Barrientos, and Antonio Largo*[a]

Abstract: First-row transition-metal dicarbides MC_2 (M = Sc–Zn) have been investigated by using quantum-mechanical techniques. The competition between cyclic and linear isomers in these systems has been studied and the bonding scheme for these compounds is discussed through topological analysis of electron density. All of the systems have been found to prefer a C_{2v}-symmetric arrangement, although for ZnC_2 the energy difference between this and the linear isomer is rather small. In most cases the C_{2v}-symmetric structure corresponds to a T-shaped structure, with the exceptions of TiC_2, CoC_2, and NiC_2 which have been shown to be true rings. A detailed analysis of the variation of the energy of the system with geometry has been carried out. An analysis of the bonding, taking into account the main interactions between the valence orbitals of both fragments, the M atom and the C_2 molecule, has allowed the main features of these compounds to be interpreted. A clear correlation between the dissociation energies of the first-row transition-metal dicarbides and the bonding energies of the corresponding met-cars was observed.

Keywords: ab initio calculations · dicarbides · dissociation energies · molecular structure · transition metals

Introduction

There is a growing interest in the interaction between transition metals and carbon. It is clearly important from the perspective of structural chemistry, but also transition-metal carbides are quite relevant in modern materials science. A wide variety of materials can be formed from the interaction of carbon with transition metals. Metallocarbohedrenes (met-cars)[1–6], with an $M_8C_{12}^+$ stoichiometry, are stable gas-phase metal–carbon cluster ions obtained from early transition metals, a prototypical example being $Ti_8C_{12}^+$. On the other hand, late transition metals have interesting properties as catalysts for carbon nanotube formation.[7] Networked metallofullerenes[8] can be formed when transition metals are incorporated into carbon cages, whereas some rare-earth elements can be trapped inside fullerene cages to form endohedral metallofullerenes.[9]

The type of structure formed depends essentially on the nature of the interaction between the transition metal and the carbon atoms. Therefore, theoretical studies of small carbon clusters containing transition metals are very useful for understanding the growth mechanisms of the various metal-carbon nanomaterials as well as for obtaining an insight into their physical and chemical properties. Transition-metal carbide clusters have quite complicated electronic structures and are also interesting subjects from the perspective of theoretical chemistry.

The smallest transition-metal carbides in which competition between different isomers can be found are clearly MC_2 (in what follows the transition metal will be denoted as M). Transition-metal dicarbides can in principle have linear or cyclic structures. Furthermore, the cyclic isomer might correspond to a true ring (with peripheral M–C bonding) or to a T-shaped structure (with M–C_2 bonding). Theoretical studies might help to shed light on the molecular structures of these species. For example, a recent theoretical study[10] of second-row (Na–Cl) dicarbides allowed the main features of these compounds to be interpreted.

A number of theoretical studies of first-row transition-metal dicarbides have been carried out,[11–24] most of them dealing with a single compound, and in all cases cyclic ground states were predicted. In addition, the atomization energies[25] and photoelectron spectra of first-row transition-

[a] Dr. V. M. Rayón, Prof. P. Redondo, Prof. C. Barrientos, Prof. A. Largo
Departamento de Química Física y Química Inorgánica
Facultad de Ciencias, Universidad de Valladolid
47005 Valladolid (Spain)
Fax: (+34) 983-423-013
E-mail: alargo@qf.uva.es

metal dicarbides have been determined experimentally.[26,27] Of particular relevance is the study of Li and Wang[27] in which the electronic structure of MC_2 compounds (M = Sc, V, Cr, Mn, Fe, and Co) based on the results of photoelectron spectra was discussed. These authors suggested that a comparison of their results with systematic theoretical studies on MC_2 compounds would be valuable to elucidate the evolution of the chemical bonding between carbon and first-row transition metals.[27] The main purpose of this work was to carry out such a systematic study across the first transition series (Sc–Zn).

Computational Methods

Two different theoretical approaches were applied to obtain the geometrical parameters. First, we carried out calculations using density functional theory (DFT) which in recent years has been extensively applied to different chemical systems owing to its reasonable performance at a relatively low cost in terms of computing time. In particular, we selected the B3LYP exchange-correlation functional[28,29] which has been widely applied to the study of many medium-sized heteroatom-doped carbon clusters, providing structures in good agreement with experimental results.[30] This consists of the Lee–Yang–Parr[31] correlation functional in conjunction with the hybrid exchange functional first proposed by Becke.[32] In addition, we have also employed the QCISD method[33] (quadratic configuration interaction including single and double excitations) which is considered to be a reliable method for predicting geometrical parameters. In both sets of calculations, B3LYP and QCISD, we employed different basis sets, but we will only report those results obtained with the basis set denoted as 6-311+G(3df). This basis set includes diffuse and polarization functions and is constructed by employing the triple split-valence 6-311G basis set[34] for carbon atoms and the Wachters–Hay[35,36] basis set with the scaling factor of Raghavachari and Trucks[37] for the first-row transition metal. Harmonic vibrational calculations were performed at both levels of theory, B3LYP and QCISD. For the B3LYP calculations we employed the 6-311+G(3df) basis set, whereas for the QCISD method we used the 6-311+G(d) basis set [at the corresponding QCISD/6-311+G(d) geometries which were found to be not too different from the 6-311+G(3df) ones]. Computation of the vibrational frequencies allowed the nature of the stationary points to be characterized, as well as an estimation of the zero-point vibrational energy (ZPVE).

The electronic energies were refined through single-point calculations on the QCISD/6-311+G(3df) geometries by employing the CCSD(T) approach[38] with the 6-311+G(3df) basis set. CCSD(T) stands for coupled-cluster single and double excitation model augmented with noniterative treatment of triple excitations. In all correlated calculations we included the valence electrons of the carbon atoms and the 4s and 3d electrons of the metal. The atomic states were obtained by following the rules given by Hay[36] for the occupation of d orbitals. All these calculations were carried out using the Gaussian 98 program package.[39]

Of course, when dealing with transition-metal compounds the possible multiconfigurational nature of the system under study is always a matter of concern. We carried out complete active space multiconfiguration self-consistent field (CASSCF) optimizations followed by multireference single and double (MRCI) single-point calculations employing the 6-311+G(d) basis set. We would like to point out that our main aim here was to check that the chosen single-reference methods (described above) provide the correct qualitative picture of the conformational preference whose analysis was one of the main goals of this work.

From a technical point of view, it is evident that it is difficult to define a unique active space for all the first-row transition-metal dicarbides taking into account the different number of d electrons involved. In principle we considered the complete active space generated by distributing all the valence electrons in 13 orbitals ($2\sigma_g$, $2\sigma_u$, $1\pi_u$, $3\sigma_g$, and $1\pi_g$ of the C_2 unit and the 4s and five 3d orbitals of the metal atom). We observed, however, that inclusion of the $3\sigma_u$ orbital of C_2 has a considerable effect on FeC_2, MnC_2, and ZnC_2. We therefore report for these species data obtained by including this orbital in the active space. In order to keep our calculations within a reasonable cost we excluded the $2\sigma_g$ orbital. In the particular case of CuC_2, the inclusion in the active space of a second $3d_{xy}$ orbital was found to have a significant effect. This is related to the double-shell effect which is particularly important for late first-row transition metals.[40,41] Data reported for this system were therefore computed with this extended active space (from which the $2\sigma_g$ orbital was again excluded). All configurations in the CASSCF with coefficients larger than 0.01 were included as reference configurations in the MRCI. The only exception was MnC_2 for which too many configurations were involved. For this system we reduced the number of references to those with coefficients larger than 0.08. We think that, for our purposes (see above), this precision is still sufficient. All these calculations were performed with the MOLPRO Version 2002.1 suite of programs.[42]

Finally, the nature of the bonding in the different C_2X species was characterized through topological analysis of their electron densities.[43] These calculations were performed with the MORPHY program[44] employing the QCISD/6-311+G(d) electron density. An analysis in terms of natural bond orbitals (NBO)[45] was also carried out.

Results and Discussion

Overview of the molecular structure of MC_2 compounds: We have searched for the lowest-lying linear and C_{2v}-symmetric states of MC_2 compounds. As expected, all linear isomers correspond to a M–C–C connectivity. Note that a C–C bond is much stronger than a M–C bond and, therefore, it is not surprising that the C–M–C isomers are found to lie much higher in energy in all cases.

Although we carried out calculations on different spin multiplicities, only the results for the lowest-lying spin state in each case will be reported. The spin multiplicity increases along the transition-metal series, starting from a doublet in the case of ScC_2 up to a sextet for the MnC_2 system. From MnC_2 the spin multiplicity decreases sequentially to the singlet state of ZnC_2. The lowest-lying states of the linear and cyclic arrangements are in agreement with previous theoretical studies (when available). The only exceptions were cyclic TiC_2 and FeC_2 and linear VC_2. In the case of TiC_2 we found a lowest-lying state corresponding to $^3B_2$ ($\cdots 9a_1^2 10a_1^1 5b_2^1$), whereas a previous combined DFT and CASSCF study[14] predicted a $^3B_1$ ($\cdots 9a_1^2 5b_2^1 1a_2^1$) lowest-lying state, although the $^3B_2$ state had a very similar energy. In our case, an energy difference between the two states of less than 1 kcal mol^{-1} was found. For the FeC_2 system we found a $^5A_2$ ($\cdots 9a_1^2 1a_2^2 5b_2^1 10a_1^1 4b_1^1 11a_1^1$) electronic lowest-lying state at the B3LYP, QCISD, and CCSD(T) levels of theory, whereas a previous study[23] predicted a $^5A_1$ ($\cdots 9a_1^2 1a_2^1 5b_2^1 10a_1^2 4b_1^1 11a_1^1$) ground state at the CASPT2 level with the $^5A_2$ state lying just 1.43 kcal mol^{-1} higher in energy. Linear VC_2 was predicted to have a sextet lowest-lying state in a previous study,[20] whereas in our calculations the quartet is slightly lower in energy. In any case, we have adopted the quartet state because it correlates with the cyclic ground state.

The geometrical parameters and vibrational frequencies for the linear isomers of the different MC_2 species are given in Table 1, whereas in Table 2 the corresponding data for the C_{2v}-symmetric structures are shown. We were not able to obtain the linear isomer of the NiC_2 system at the QCISD level of theory owing to convergence problems in the optimization procedure. Therefore, in what follows all QCISD or CCSD(T) results obtained for linear NiC_2 were obtained from the B3LYP geometry. The data collected in Table 1 show the following trend in the M–C bond distances: B3LYP < QCISD < CASSCF. In general, reasonable agreement can be observed between the three sets of geometrical parameters, especially for the C–C distances. In some cases, CASSCF geometries have significantly larger M–C bond distances than B3LYP and QCISD geometries. This happens in the middle of the series for the linear isomers (Cr–Co) and somewhat later in the series for the cyclic ones (Co and Ni) and must be partially related to the multireference character of the wavefunctions of these particular systems which show non-negligible contributions from con-

Table 1. Electronic configurations, geometrical parameters, and harmonic vibrational frequencies for linear MC_2 species obtained by the B3LYP/6-311+G(3df), QCISD/6-311+G(3df) (second line), and CASSCF/6-311+G(d) (in parentheses) methods. QCISD vibrational frequencies were computed using the 6-311+G(d) basis set.

Linear MC_2	Electronic configuration	Linear geometry [Å]				Vibrational frequencies [cm^{-1}]
		R(M–C)		R(C–C)		
ScC_2 ($^2\Sigma$)	{core}$8\sigma^2 9\sigma^2 3\pi^4 10\sigma^2 11\sigma^1$	1.906	(1.935)	1.275	(1.299)	103i(π), 605(σ), 1869(σ)
		1.928		1.278		112i(π), 597(σ), 1813(σ)
TiC_2 ($^3\Delta$)	{core}$8\sigma^2 9\sigma^2 3\pi^4 10\sigma^2 11\sigma^1 1\delta^1$	1.860	(1.884)	1.276	(1.304)	94i(π), 601(σ), 1859(σ)
		1.884		1.279		247(π), 574(σ), 1799(σ)
VC_2 ($^4\Sigma$)	{core}$8\sigma^2 9\sigma^2 3\pi^4 10\sigma^2 1\delta^2 11\sigma^1$	1.840	(1.881)	1.279	(1.288)	97i(π), 573(σ), 1838(σ)
		1.880		1.279		802(π), 498(σ), 1743(σ)
CrC_2 ($^5\prod$)[a]	{core}$8\sigma^2 9\sigma^2 3\pi^4 10\sigma^2 1\delta^2 11\sigma^1 4\pi^1$	1.891	(2.121)	1.286	(1.255)	220i(π), 164(π), 452(σ), 1792(σ)
		1.940		1.298		228i(π), 166(π), 391(σ), 1755(σ)
MnC_2 ($^6\Sigma$)	{core}$8\sigma^2 9\sigma^2 3\pi^4 10\sigma^2 1\delta^2 11\sigma^1 4\pi^2$	1.824	(2.131)	1.269	(1.253)	95(π), 527(σ), 1806(σ)
		1.892		1.266		211(π), 657(σ), 1856(σ)
FeC_2 ($^5\Delta$)	{core}$8\sigma^2 9\sigma^2 3\pi^4 10\sigma^2 1\delta^3 11\sigma^1 4\pi^2$	1.779	(2.078)	1.275	(1.252)	117(π), 568(σ), 1805(σ)
		1.834		1.262		191(π), 681(σ), 1894(σ)
CoC_2($^4\Delta$)	{core}$8\sigma^2 9\sigma^2 3\pi^4 10\sigma^2 11\sigma^2 1\delta^3 4\pi^2$	1.746	(2.015)	1.287	(1.255)	68(π), 585(σ), 1760(σ)
		1.856		1.255		262(π), 945(σ), 1876(σ)
NiC_2($^3\Sigma$)	{core}$8\sigma^2 9\sigma^2 3\pi^4 1\delta^4 10\sigma^2 11\sigma^2 4\pi^2$	1.733	(1.945)	1.294	(1.254)	48(π), 545(σ), 1738(σ)
		–		–		–
CuC_2($^2\Sigma$)	{core}$8\sigma^2 9\sigma^2 3\pi^4 10\sigma^2 1\delta^4 4\pi^4 11\sigma^1$	1.836	(1.878)	1.223	(1.240)	277i(π), 483(σ), 2038(σ)
		1.856		1.231		79(π), 483(σ), 2006(σ)
ZnC_2($^1\Sigma$)	{core}$8\sigma^2 9\sigma^2 3\pi^4 1\delta^4 10\sigma^2 4\pi^4 11\sigma^2$	1.848	(1.971)	1.249	(1.248)	108(π), 491(σ), 1926(σ)
		1.899		1.224		95i(π), 535(σ), 1992(σ)

[a] Note that nondegenerate π vibrational frequencies corresponding to the two Renner–Teller components were obtained for this state.

Table 2. Electronic configurations, geometrical parameters, and harmonic vibrational frequencies for cyclic MC_2 species obtained by the B3LYP/6-311+G(3df), QCISD/6-311+G(3df) (second line), and CASSCF/6-311+G(d) (in parentheses) methods. QCISD vibrational frequencies were computed with the 6-311+G(d) basis set.

Cyclic MC_2	Electronic configuration	Cyclic geometry [Å, degrees]						Vibrational frequencies [cm^{-1}]
		R(M–C)		R(C–C)		∢CMC		
ScC_2 ($^2A_1$)	{core}$7a_1^2 4b_2^2 8a_1^2 3b_1^2 9a_1^2 10a_1^1$	2.061	(2.083)	1.261	(1.289)	35.6	(36.0)	331(b_2), 634(a_1), 1832(a_1)
		2.073		1.267		35.6		344(b_2), 641(a_1), 1812(a_1)
TiC_2 ($^3B_2$)	{core}$7a_1^2 4b_2^2 8a_1^2 3b_1^2 9a_1^2 10a_1^1 5b_2^1$	1.984	(2.080)	1.283	(1.281)	37.7	(35.9)	173(b_2), 581(a_1), 1704(a_1)
		2.026		1.283		36.9		772(b_2), 548(a_1), 1716(a_1)
VC_2 ($^4B_1$)	{core}$7a_1^2 4b_2^2 8a_1^2 3b_1^2 9a_1^2 1a_1^1 5b_2^1 10a_1^1$	1.933	(2.032)	1.286	(1.282)	38.9	(36.8)	378(b_2), 575(a_1), 1693(a_1)
		1.960		1.288		38.3		890(b_2), 548(a_1), 1698(a_1)
CrC_2 ($^5A_1$)	{core}$7a_1^2 4b_2^2 8a_1^2 3b_1^2 9a_1^2 1a_1^1 5b_2^1 10a_1^1 4b_1^1$	1.985	(2.066)	1.273	(1.279)	37.4	(36.1)	364(b_2), 483(a_1), 1763(a_1)
		1.991		1.277		37.4		852(b_2), 522(a_1), 1774(a_1)
MnC_2 ($^6A_1$)	{core}$7a_1^2 4b_2^2 8a_1^2 3b_1^2 9a_1^2 1a_1^1 5b_2^1 10a_1^1 4b_1^1 11a_1^1$	1.979	(2.073)	1.273	(1.293)	37.5	(36.3)	366(b_2), 568(a_1), 1759(a_1)
		2.031		1.273		36.5		371(b_2), 495(a_1), 1767(a_1)
FeC_2 ($^5A_2$)	{core}$7a_1^2 4b_2^2 8a_1^2 3b_1^2 9a_1^2 1a_1^2 5b_2^1 10a_1^1 4b_1^1 11a_1^1$	1.922	(2.044)	1.276	(1.277)	38.8	(36.4)	428(b_2), 578(a_1), 1747(a_1)
		1.947		1.274		38.2		432(b_2), 533(a_1), 1788(a_1)
CoC_2 ($^4B_1$)	{core}$7a_1^2 4b_2^2 8a_1^2 3b_1^2 9a_1^2 1a_1^2 5b_2^2 10a_1^1 4b_1^1 11a_1^1$	1.874	(2.026)	1.298	(1.279)	40.5	(36.8)	519(b_2), 550(a_1), 1641(a_1)
		1.902		1.298		39.9		387(b_2), 470(a_1), 1695(a_1)
NiC_2 ($^3B_1$)	{core}$7a_1^2 4b_2^2 8a_1^2 3b_1^2 9a_1^2 1a_1^2 5b_2^2 10a_1^2 4b_1^1 11a_1^1$	1.871	(2.006)	1.295	(1.281)	40.5	(37.2)	405(b_2), 517(a_1), 1662(a_1)
		1.861		1.309		41.2		429(b_2), 538(a_1), 1602(a_1)
CuC_2 ($^2A_1$)	{core}$7a_1^2 4b_2^2 8a_1^2 3b_1^2 9a_1^2 1a_1^2 5b_2^2 10a_1^2 4b_1^2 11a_1^1$	1.976	(2.090)	1.278	(1.284)	37.7	(35.8)	292(b_2), 437(a_1), 1750(a_1)
		1.994		1.285		37.6		293(b_2), 419(a_1), 1710(a_1)
ZnC_2 ($^1A_1$)	{core}$7a_1^2 4b_2^2 8a_1^2 3b_1^2 9a_1^2 1a_1^2 5b_2^2 10a_1^2 4b_1^2 11a_1^2$	1.976	(2.094)	1.277	(1.273)	37.7	(35.4)	304(b_2), 511(a_1), 1705(a_1)
		2.034		1.270		36.4		293(b_2), 362(a_1), 1814(a_1)

figurations other than the leading one. The wavefunctions of the two isomers of ZnC_2 also have some multireference character. The rest of the systems are highly single-determinantal. In order to obtain more precise geometries it would be necessary to include the dynamic electron correlation not recovered in the MCSCF treatment. This is a computationally demanding task which is beyond the scope of this study. We would like to point out that the differences in the metal–carbon bond distances across the series Sc–Zn are not really large: for the linear isomers, for example, the longest bond is Cr–C, 1.940 Å, and the shortest Fe–C, 1.834 Å (QCISD level). Thus, all M–C bond distances in the linear isomers lie within 0.1 Å, whereas in the cyclic isomers they lie within 0.2 Å. Taking into account the fact that there should be several factors that contribute to the observed bond distances (size of the metal atoms, amount of charge donation, metal–ligand repulsion, etc.), we must be careful when trying to explain such small differences. The C–C distances are quite similar for the cyclic isomers, varying in the range of 1.267–1.309 Å (QCISD level) and corresponding to values that can be classified as intermediate between typical C–C double and triple bonds. As a reference, the C–C distance in the C_2 molecule is 1.247 Å (B3LYP), 1.250 Å (QCISD), or 1.254 Å (CASSCF). In the case of the linear isomers the C–C distances are in the range of 1.224–1.298 Å. In most cases the C–C distance increases with respect to that found in C_2, the only exceptions being CuC_2 and ZnC_2 in which a noticeable shortening is found.

For the cyclic isomers, there are some important quantitative differences between the vibrational frequencies computed at the B3LYP and QCISD levels of theory, especially for the b_2 normal mode of TiC_2, VC_2, and CrC_2, and also for the C–C stretching frequency of ZnC_2. Nevertheless, in general the vibrational frequencies computed at both levels of theory are in reasonable agreement. However, in the case of the linear isomers, the discrepancies between the two sets of vibrational frequencies are certainly more important because there are some qualitative differences. For three different dicarbides (TiC_2, VC_2, and CuC_2) the linear isomers have an imaginary π vibrational frequency at the B3LYP level of theory, whereas the QCISD level provides all real frequencies. Therefore, these structures are transition states for the degenerate rearrangement of the C_{2v}-symmetric species at the B3LYP level of theory, whereas they are true minima at the QCISD level. Another discrepancy is observed for linear ZnC_2; the B3LYP method predicts a true minimum, whereas at the QCISD level this species has an imaginary frequency. For the rest of the dicarbides both levels of theory agree on the nature of the linear isomer, namely a transition state for ScC_2 and true minima in all other cases.

To characterize the type of interaction between the transition metal and the carbon atoms, as well as the bonding scheme in MC_2 compounds, we carried out a topological analysis of the electronic charge density.[43] Critical points in the one-electron density, $\rho(r)$, computed at the QCISD/6-311+G(d) level of theory were identified. In the case of the MC_2 systems only bond critical points[43] [corresponding to a minimum value of $\rho(r)$ along the line linking the nuclei and a maximum along the interatomic surfaces] and ring critical points[43] [$\rho(r)$ being a minimum in two directions and a maximum in one direction] are relevant. Only the most important properties of the critical points, namely the electron density, $\rho(r)$, at the critical point, the Laplacian of the charge density, $\nabla^2\rho(r)$, and the total energy density, $H(r)$, will be discussed. The chemical nature of the bonding can be determined according to the values of the charge density and its Laplacian at the bond critical point. There are basically two limiting types of atomic interactions, namely shared and closed-shell interactions.[43] Nevertheless, there is a whole spectrum of intermediate interactions lying between these two extreme cases.[46]

Shared interactions are in general characterized by large electron densities and negative values of the Laplacian[43] and are characteristic of covalent compounds. On the other hand, closed-shell interactions correspond to relatively low $\rho(r)$ and positive values of $\nabla^2\rho(r)$,[43] a situation which is usually found for ionic and van der Waals compounds. In many cases the total energy density, $H(r)$, which is the sum of the potential and kinetic energy densities at a critical point, might be useful in order to characterize the degree of covalency of a bond. If $H(r)<0$ the system is stabilized by the accumulation of electronic charge in the internuclear region, the characteristics of a covalent interaction.[47] Conversely, if $H(r)$ is positive, accumulation of electronic charge would lead to a destabilization of the system, a typical feature of van der Waals and ionic bonding systems. A summary of critical point data, such as the $\rho(r)$, $\nabla^2\rho(r)$, and $H(r)$ values at the bond critical points obtained with the QCISD/6-311+G(d) electron density, is given in Table 3. It is readily seen in Table 3 that most of the C_{2v}-symmetric isomers have a C–C bond critical point, as well as a bond critical point between the transition metal and the midpoint of the C_2 unit. Therefore, these species are in fact T-shaped compounds rather than truly cyclic molecules since there is no ring critical point. The only exceptions are TiC_2, CoC_2, and NiC_2 for which topological analysis of the electron density of the C_{2v}-symmetric species allows two individual M–C bond critical points to be characterized along with a ring critical point. Therefore, in principle these three C_{2v}-symmetric compounds should be classified as truly cyclic species. Nevertheless, it should be pointed out that for cyclic CoC_2 and NiC_2, the M–C bonds are rather curved with the M–C bond critical points quite close to the ring critical points [the values of $\rho(r)$ at the ring critical points are 0.1177 and 0.1284 a.u., respectively, and therefore very close to the $\rho(r)$ values at the M–C critical points], indicating that these species are not far from being T-shaped. In particular, for cyclic TiC_2, the electron density at the ring and bond critical points is virtually the same, namely 0.1017, suggesting that this structure, although nominally a ring, approaches a T-shaped description.

According to the data shown in Table 3, all linear isomers have M–C bonds corresponding to intermediate interac-

Table 3. Summary of the critical point data for the linear and cyclic isomers of MC_2 species, using the QCISD/6-311+G(d) electronic density (in a.u.).

Isomer	Bond		Sc	Ti	V	Cr	Mn	Fe	Co	Ni	Cu	Zn
linear	M–C	$\rho(r)$	0.139	0.147	0.138	0.103	0.125	0.143	0.152	0.174	0.123	0.115
		$\nabla^2\rho(r)$	0.194	0.178	0.224	0.434	0.319	0.381	0.443	0.440	0.372	0.333
		$-H(r)$	0.116	0.122	0.123	0.132	0.131	0.158	0.173	0.197	0.138	0.125
	C–C	$\rho(r)$	0.371	0.367	0.366	0.367	0.370	0.372	0.429	0.361	0.356	0.379
		$\nabla^2\rho(r)$	−1.204	−1.174	−1.169	−1.175	−1.139	−1.182	−1.701	−1.137	−0.932	−1.121
		$-H(r)$	0.179	0.180	0.180	0.172	0.205	0.195	0.203	0.176	0.255	0.265
cyclic	M–C_2	$\rho(r)$	0.099		0.115	0.103	0.091	0.110			0.093	0.084
		$\nabla^2\rho(r)$	0.281		0.368	0.320	0.339	0.383			0.309	0.268
		$-H(r)$	0.100		0.132	0.111	0.106	0.129			0.105	0.091
	M–C	$\rho(r)$		0.102					0.119	0.130		
		$\nabla^2\rho(r)$		0.342					0.386	0.405		
		$-H(r)$		0.117					0.138	0.152		
	C–C	$\rho(r)$	0.375	0.358	0.354	0.353	0.368	0.365	0.345	0.332	0.333	0.351
		$\nabla^2\rho(r)$	−1.121	−1.013	−0.990	−0.977	−1.090	−1.063	−0.969	−0.891	−0.858	−0.962
		$-H(r)$	0.220	0.207	0.204	0.211	0.209	0.212	0.190	0.181	0.200	0.216

tions. They have some of the characteristics of ionic bonds, such as the positive values of the Laplacian of $\rho(r)$ (compared with the corresponding negative values of C–C bond critical points typical of covalent interactions). However, although the values of $\rho(r)$ are rather small, they are always greater than 0.1 a.u. This fact, together with the negative values of $H(r)$ for all the M–C bonds, indicating a certain degree of covalency, suggests that the M–C interactions can be classified as intermediate ones. For the C_{2v}-symmetric species similar behavior is generally observed. In general, in these species the M–C bonds have lower values of $\rho(r)$, as well as less negative $H(r)$ values, than linear isomers, suggesting greater ionic character.

Atomic charges, obtained through a natural bond orbital (NBO)[45] analysis at the QCISD/6-311+G(3df) level of theory, are given in Table 4. As can be seen in Table 4, most of the linear and cyclic MC_2 compounds have a net atomic charge at the metal atom close to $+1e$ (with the exception of linear CrC_2 and NiC_2). Although NBO charges should be regarded with caution for transition-metal compounds,[48] it is clear that the NBO results suggest a net transfer of one electron from the transition metal to the C_2 unit.

Variation of energy with the geometry of MC_2 compounds: One of the most interesting features of transition-metal dicarbides is the competition between linear and C_{2v}-symmetric isomers. The energy differences between the two isomers at the four levels of theory employed in this work, including ZPVE corrections, are given in Table 5.

Regarding the results obtained by single-reference methods, there is in general a reasonable agreement between the QCISD and CCSD(T) levels, the only exception being for CoC_2 for which a discrepancy of about 10 kcal mol^{-1} between the two levels of theory is observed. The B3LYP results differ from the CCSD(T) ones by about 1–5 kcal mol^{-1} in most cases, with the exception of CrC_2 and CoC_2. Nevertheless, note that all levels of theory agree in the order of stability of the linear and C_{2v}-symmetric isomers. The relative energies at the MRCI level of theory are also shown in Table 5. Note here that in the particular cases of CrC_2, MnC_2, FeC_2, and NiC_2 the discrepancies between the CASSCF and B3LYP/QCISD geometrical parameters are significantly different for the cyclic and the linear isomers

Table 5. Relative energies ($E_{cyclic}-E_{linear}$) of the cyclic MC_2 species at different levels of theory with the 6-311+G(3df) basis set and including ZPVE corrections. For the QCISD, CCSD(T), and MRCI calculations, QCISD/6-311+G(d) ZPVE values were employed.

MC_2	Relative energy [kcal mol^{-1}]			
	B3LYP	QCISD	CCSD(T)	MRCI
ScC_2	−15.78	−18.88	−18.27	−15.66
TiC_2	−14.35	−18.69	−18.41	−11.15
VC_2	−19.43	−25.26	−25.72	−19.77
CrC_2	−11.39	−18.54	−22.14	−15.52[a]
MnC_2	−9.95	−15.87	−14.83	−20.09[a]
FeC_2	−12.24	−15.88	−17.87	−19.76[a]
CoC_2	−10.86	−10.16	−20.49	−20.18
NiC_2	−12.64	–	−13.39	−11.85[b]
CuC_2	−5.52	−4.58	−6.78	−5.18
ZnC_2	−6.33	−2.99	−1.15	+1.82

[a] QCISD/6-311+G(3df) geometries, see text. [b] B3LYP/6-311+G(3df) geometry, see text.

Table 4. NBO atomic charges obtained at the QCISD/6-311+G(3df) level of theory.

Isomer	Atomic charge	Sc	Ti	V	Cr	Mn	Fe	Co	Ni	Cu	Zn
linear	Q(M)	1.226	0.990	0.917	0.697	1.226	1.016	0.728	0.561	0.779	0.911
	$Q(C_1)$	−1.212	−0.998	−0.930	−0.591	−1.200	−0.919	−0.855	−0.695	−0.843	−1.023
	$Q(C_2)$	−0.014	0.008	0.013	−0.112	−0.026	0.147	0.127	0.134	0.064	0.112
cyclic	Q(M)	1.192	1.158	1.012	1.037	1.157	1.016	0.834	0.783	0.838	0.932
	Q(C)	−0.596	−0.579	−0.506	−0.518	−0.578	−0.508	−0.417	−0.392	−0.419	0.466

(see Table 1 and Table 2). For these species we would not therefore expect an agreement between the MRCI- and single-reference-based energies. Thus, in these cases we decided to use the QCISD/6-311+G(3df) (for CrC_2, MnC_2, and FeC_2) and B3LYP/6-311+G(3df) (for NiC_2) geometries in the MRCI calculations. The MRCI data collected in Table 5 nicely support the relative energies obtained by single-reference methods. For the late transition-metal dicarbides (Fe–Zn) the difference in energy with respect to the CCSD(T) level is actually less than 3 kcal mol^{-1}. For the early transition-metal species differences between 3–7 kcal mol^{-1} are found. The most important conclusion from the results shown in Table 5 is that for all the dicarbides the C_{2v}-symmetric species is more stable than the linear one. The energy differences are high enough to be confident in this conclusion, perhaps with ZnC_2 as the only exception. Although there are oscillations in the relative energies along the transition-metal series, in general it is observed that the relative energies of the linear and cyclic isomers decrease for the late transition metals.

To gain a deeper understanding of the competition between linear and cyclic isomers, we analyzed the variation of the total energy with the geometry of the system. The variation in the energy (relative to the linear isomer) as a function of the angle (φ) between the line connecting the transition-metal atom M to the midpoint of the C–C bond for the different MC_2 species is shown in Figure 1a (Sc–Mn) and Figure 1b (Fe–Zn). In these representations the linear isomer is placed at $\varphi=0$ and $\varphi=180$, whereas the C_{2v}-symmetric structure corresponds to $\varphi=90$. The curves were obtained by optimizing the C–C and M–(C–C) distances for various fixed φ angles at the B3LYP/6-311+G(d) level of theory followed by single-point CCSD(T)/6-311+G(d) calculations at each geometry.

It is readily seen in Figure 1 that the energy decreases monotonically from the linear arrangement to the C_{2v} configuration for only scandium, chromium, and copper, thus suggesting that at the CCSD(T) level of theory it is quite likely that the linear species for these systems is not a true minimum. In all other cases the energy increases as the system deviates from the linear arrangement, passes through a maximum (which could be taken as an approximation at that level of theory to the transition state connecting the $C_{\infty v}$ and C_{2v} structures), and then drops to the C_{2v} minimum. Therefore, only in two cases, namely copper and zinc, are the CCSD(T)/6-311+G(d)//B3LYP/6-311+G(d) calculations in disagreement with the predicted nature of the linear isomer at the QCISD/6-311+G(d) level of theory. According to the results shown in Table 1, the QCISD level predicts that the linear CuC_2 isomer is a true minimum, whereas linear ZnC_2 has an imaginary frequency and therefore corresponds to a transition state. The approximate barriers to linear–cyclic conversion in those cases in which the linear species is a minimum are relatively low in all cases (especially for FeC_2 and MnC_2), with values in the range of 1–7 kcal mol^{-1}. Only for VC_2 is a value higher than 10 kcal mol^{-1} observed.

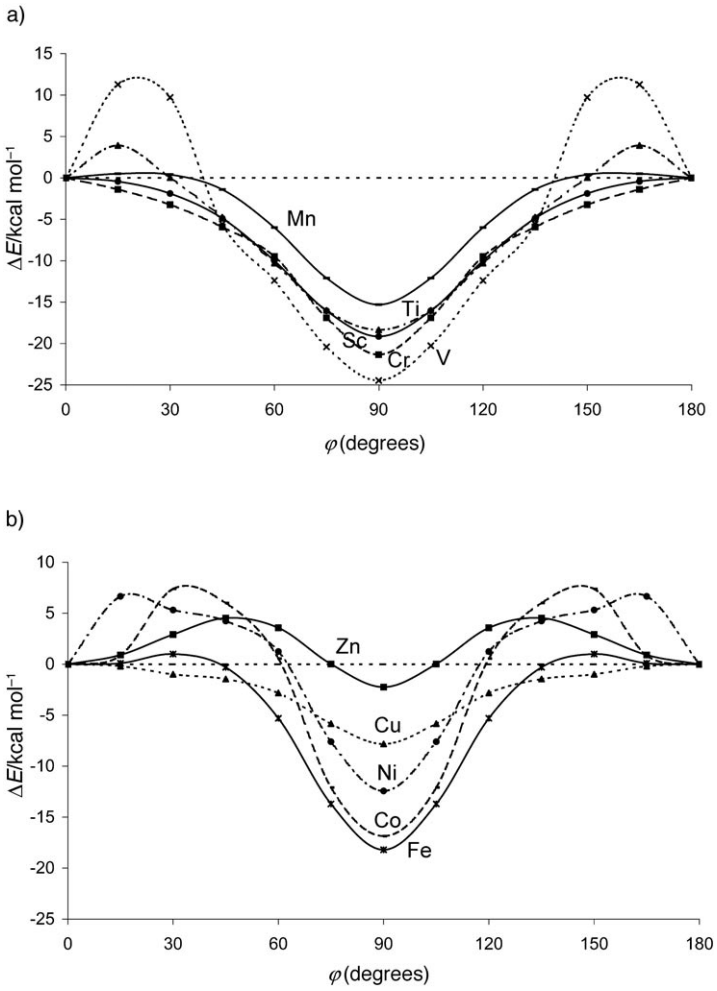

Figure 1. Variation of the total energy (in kcal mol^{-1}, relative to the linear geometry), computed at the CCSD(T)/6-311+G(d) level, for the different MC_2 compounds with the angle (φ) between the line connecting the M atom and the midpoint of the C–C bond. a) For the early transition metals (Sc–Mn); b) for the late transition metals (Fe–Zn).

For early transition metals (Sc–Mn) the energy separation between the C_{2v} and linear species oscillates along the series and is relatively high and of roughly similar magnitude for all of them, within the range of 15–25 kcal mol^{-1}. On the other hand, for late first-row transition metals it can be seen that the energy difference between the C_{2v} and linear isomers (the depth of the well in Figure 1b) decreases along the series Fe-Co-Ni-Cu-Zn, which is almost the same order as found at the CCSD(T)/6-311+G(3df) level of theory (Table 5). Furthermore, the energy difference between the two species becomes much smaller for the last member of the series. It decreases from a value of nearly 18 kcal mol^{-1} for iron to a value of just 2 kcal mol^{-1} for zinc. In fact, for ZnC_2 it is observed that the energy varies smoothly with φ angle. Therefore, ZnC_2 very much resembles a polytopic system,[49] that is, a system with a very flat potential surface. The concept of polytopism, first introduced by Clementi et al.[49] when studying the very flat potential surface of lithium cyanide, reflects the pinwheel motion of an atom (or

ion) around a molecular fragment. In our previous study of second-row dicarbides,[10] we observed similar polytopic behavior for some dicarbides with strong ionic character, for example, NaC_2, MgC_2, and AlC_2. In the case of SiC_2[10] its polytopic character was particularly evident as a consequence of a balance between ionic interactions, which favor the cyclic species, and covalent interactions,[10] resulting in a very flat surface.

Finally, we also computed the dissociation energies of the two isomers. Dissociation energies for the $MC_2 \rightarrow M+C_2$ process were computed at the B3LYP and CCSD(T) levels of theory and included ZPVE corrections. The results are given in Table 6. It is readily seen that for all systems, with the exception of CrC_2, there is a poor agreement between the dissociation energies obtained at the two levels of theory. The disagreement can mainly be attributed to the poor description of the energetics of the C_2 system at the B3LYP level of theory. In fact, the B3LYP level predicts that the ground state of C_2 should be the $^3\prod_u$ state with the $^1\Sigma_g^+$ state lying about 23 kcal mol^{-1} higher in energy. Correlation effects seem important for properly describing this system, as has been emphasized in recent theoretical studies.[50,51] In our case, the CCSD(T) level predicts the singlet to be about 2 kcal mol^{-1} below the triplet. If this discrepancy for C_2 was taken into account, which amounts to nearly 25 kcal mol^{-1}, the two sets of dissociation energies would be much closer.

Table 6. Dissociation energies (kcal mol^{-1}) of the linear and cyclic MC_2 species at the B3LYP and CCSD(T) levels of theory, including ZPVE corrections, with the 6-311+G(3df) basis set. For the CCSD(T) calculations, QCISD/6-311+G(d) ZPVE values were employed.

MC_2	Dissociation energy [kcal mol^{-1}]			
	linear		cyclic	
	B3LYP	CCSD(T)	B3LYP	CCSD(T)
ScC_2	143.46	107.71	159.24	125.98
TiC_2	140.24	99.61	154.59	118.02
VC_2	135.03	92.82	154.46	118.54
CrC_2	85.21	74.97	96.60	97.11
MnC_2	109.54	72.50	119.49	87.33
FeC_2	115.77	77.88	128.00	95.75
CoC_2	113.83	74.15	124.69	94.90
NiC_2	107.38	85.43	120.02	98.82
CuC_2	101.97	78.81	107.49	85.59
ZnC_2	67.96	53.75	74.29	54.96

The case of CrC_2 (with a quintet ground state) is special because its dissociation energy was computed relative to the $Cr(^7S)+C_2(^3\prod_u)$ dissociation limit in order to conserve the spin multiplicity. In this case a relatively good agreement was obtained for the dissociation energies at the B3LYP and CCSD(T) levels of theory. Therefore, we can conclude that, even though there are important quantitative differences between the B3LYP and CCSD(T) dissociation energies, the qualitative agreement between the two levels of theory is good.

With the exceptions of a relatively low value for MnC_2 and perhaps a slightly high value for NiC_2, the stability of the dicarbides is higher for the early than for the late first-row transition metals. The general trend observed in the CCSD(T) values, which is also evident in the B3LYP results, is that the dissociation energy decreases as one moves from the left to the right of the Periodic Table for both linear and cyclic isomers. First, the dissociation energy decreases slightly from ScC_2 to VC_2, then it drops down for CrC_2 (about 20 kcal mol^{-1}) where it remains more or less constant until ZnC_2, where it drops again about 30 kcal mol^{-1}.

Analysis of the bonding in first-row transition-metal dicarbides: In this section we will try to analyze in detail the bonding in first-row transition-metal dicarbides in order to understand more deeply their molecular structure and stability.

Given the electronic configuration of the C_2 fragment in its $^1\Sigma_g^+$ electronic state ($1\sigma_g^2 1\sigma_u^2 2\sigma_g^2 2\sigma_u^2 1\pi_u^4$), the relevant molecular orbitals that can interact with the valence orbitals of the transition metal are the $1\pi_u$ (HOMO), $3\sigma_g$ (LUMO), and $1\pi_g$ (next-LUMO) orbitals. The main interactions are depicted schematically in Figure 2 (C_{2v} symmetry) and Figure 3 ($C_{\infty v}$ symmetry). Although the bonding in these molecules involves electrostatic, covalent, and dative contributions, when discussed in terms of the dissociating (neu-

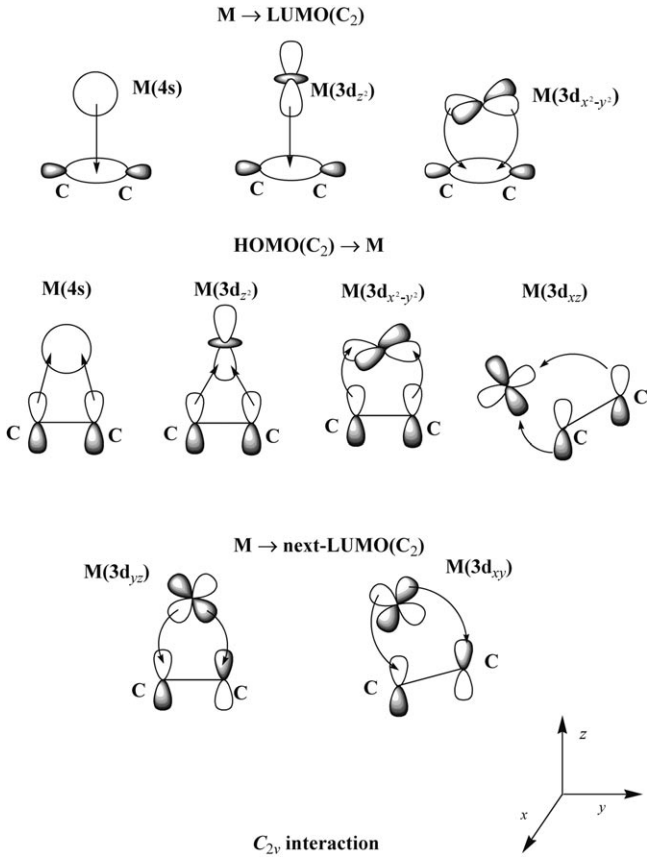

Figure 2. Schematic representation of the main interactions between the valence orbitals of the M and C_2 fragments in C_{2v} symmetry.

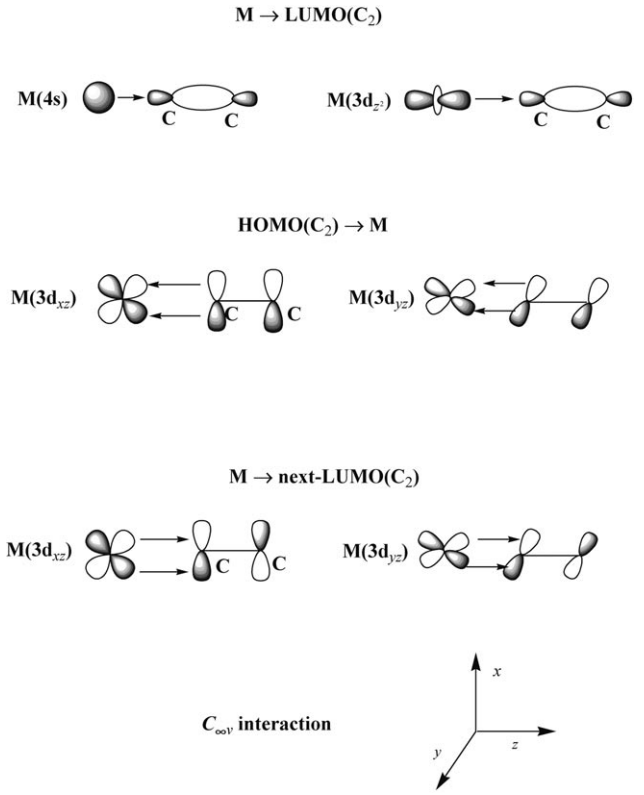

Figure 3. Schematic representation of the main interactions between the valence orbitals of the M and C_2 fragments in $C_{\infty v}$ symmetry.

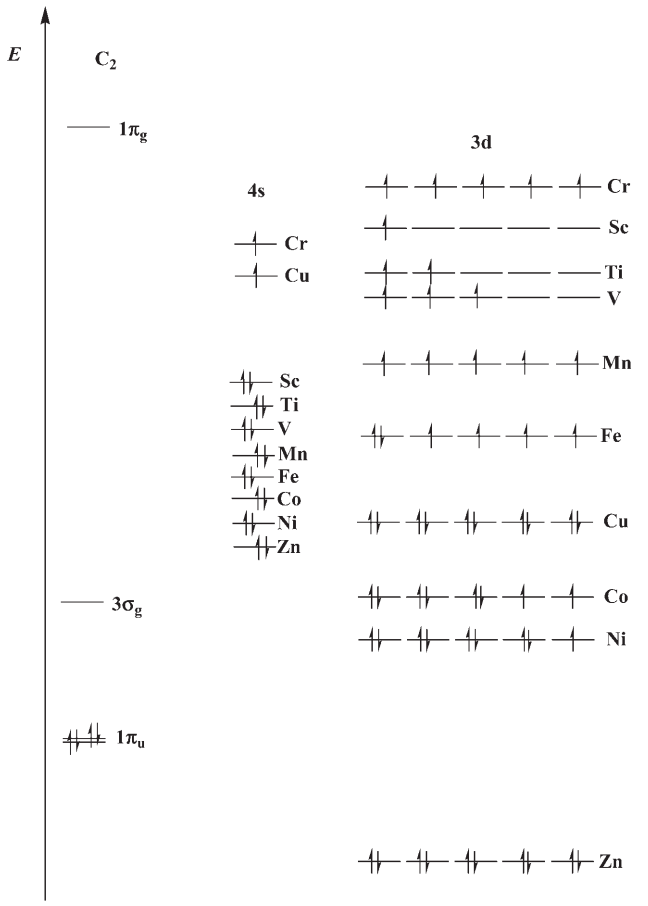

Figure 4. Schematic representation of the relative disposition and occupation of the relevant orbitals of the M and C_2 fragments.

tral) fragments, M and C_2 ($^1\Sigma_g^+$ or $^3\prod_u$), the metal–ligand bond can formally be described in terms of donor–acceptor interactions which can be classified into three different categories: 1) M→LUMO(C_2) donation, 2) M←HOMO(C_2) back-donation, and 3) M→next-LUMO(C_2) donation. Of course, which interactions are predominant in each case is dictated essentially by the relative energies of the corresponding interacting orbitals as well as by the occupation numbers of such orbitals. A schematic representation of the occupation of the orbitals of the different first-row transition metals is depicted in Figure 4.

In the linear species, donation from the metal to the LUMO of C_2 can be accomplished mainly by the 4s electrons (the 4s orbital can hybridize with the $3d_{z^2}$ orbital which also has the appropriate σ symmetry). In the cyclic species the LUMO and one of the HOMOs of C_2 have σ (a_1) symmetry. These orbitals will mainly interact with the 4s and $3d_{z^2}$ orbitals of the metal, although interaction with the $3d_{x^2-y^2}$ orbital is also possible. Back-donation can also take place from the second HOMO of C_2 in the b_1 representation. Further stabilization is achieved by mixing the next-LUMOs of C_2, which are the antibonding π* orbitals, with the corresponding atomic orbitals of the metal. In the linear species this happens in the π representation, whereas in the cyclic species the next-LUMOs belong to the a_2 and b_2 representations.

In principle, from the schematic representation of Figure 4, one can anticipate that the dominant interaction for all first-row transition-metal dicarbides is M(4s)→LUMO(C_2) donation. It seems that this interaction should be slightly more favorable in the C_{2v}-symmetric than in the linear geometries owing to the larger overlap between the corresponding orbitals and this would explain in part the preference for the C_{2v}-symmetric arrangement. This donation from the metal would be responsible for much of the net positive charge at the transition metal. Furthermore, for the C_{2v} isomers, the M(4s,$3d_{z^2}$)→LUMO(C_2) donation takes place mainly along the line connecting the metal to the midpoint of the C–C bond, thus favoring in general T-shaped structures.

We will begin by briefly describing the bonding situation in the linear first-row transition-metal dicarbides. The electronic state of ScC_2 is $^2\Sigma$ which gives us the following scandium d orbital occupation: $4s^2 3d_{z^2}^1$. The 4s and $3d_{z^2}$ orbitals can mix to yield two new hybrid orbitals. One of the hybrids points directly towards the C_2 fragment whereas the other one removes electron density from the σ region creating a torus of density around the molecular axes. The first hybrid will be doubly occupied because this is the orbital that donates density into the LUMO of C_2. Besides, the 3dπ orbitals of the metal ($3d_{xz}$ and $3d_{yz}$) are empty and will thus mix with the π HOMOs of the C_2 fragment. In the $^2\Delta$ state of

ScC_2 the unpaired electron goes into one of the nonbonding 3dδ ($3d_{xy}$, $3d_{x2-y2}$) orbitals. This state lies about 13 kcal mol^{-1} above the $^2\Sigma$ state. On the other hand, the $^2\prod$ state will lie at an even higher energy (about 21 kcal mol^{-1} above $^2\Sigma$) because the unpaired electron occupies an antibonding π orbital. This qualitative description of the Sc–C_2 interaction actually shows the underlying contributions that explain the bonding situation in the linear metal dicarbides, that is, donation from the 4s+$3d_{z^2}$ hybrid orbital into the LUMO of C_2, back-donation from the two degenerate HOMOs of C_2 into the 3dπ orbitals of the metal, and occupation of the 3dδ and 4s–$3d_{z^2}$ hybrid orbitals by the nonbonding transition-metal electrons.

In line with this, for TiC_2 and VC_2 the extra electrons add to the nonbonding 3dδ orbitals leading to the $^3\Delta$ and $^4\Sigma$ states, respectively. The bonding situation in ScC_2, TiC_2, and VC_2 is therefore similar: one (dative) two-electron σ bond and two (also dative) two-electron π bonds with nonbonding electrons occupying the 3dδ orbitals. It is therefore not surprising that these three molecules have similar bond distances and dissociation energies. We can tentatively attribute the shortening of the metal–ligand bond distance when going from scandium to vanadium simply to the decrease in the atom size.

In CrC_2, the bonding can be seen as arising from the mixture of these two asymptotes: $4s^13d^5(3d_\sigma{}^13d_\pi{}^23d_\delta{}^2)+C_2(^3\prod_u)$ and $4s^23d^4(3d_\sigma{}^13d_\pi{}^13d_\delta{}^2)+C_2(^1\Sigma_g{}^+)$. As the energy required to excite C_2 to the triplet first-excited state is much smaller than the first excitation energy of chromium, the first asymptote will dominate. This picture of the bonding explains the long C–C distance and its low stretching frequency (see Table 1). It also explains the relatively large spin polarization in the σ bond for this molecule: the net β spin density of the carbon atom attached to chromium is −0.4 whereas the chromium α spin density is 4.5. This spin polarization can also be seen in the different fragment contributions to the α and β MOs. The spin polarization in the σ Cr–C bond must be related to the increase in the metal–carbon bond length in this system as well as to the decrease in its dissociation energy.

In MnC_2, the extra electron adds formally to the M–C_2 π antibonding orbital which was already singly occupied in CrC_2. Therefore a shorter C–C bond distance and a higher C–C stretching frequency are found in this molecule.

In FeC_2, CoC_2, and NiC_2, electrons add in turn to the δ, σ, and δ transition-metal orbitals leading to the $^5\Delta$, $^4\Delta$, and $^3\Sigma$ states, respectively. Nevertheless, for FeC_2 and CoC_2 the $^5\Sigma$ and $^4\Sigma$ states (resulting from addition of electrons to the σ and δ orbitals) are very close in energy to the $^5\Delta$ and $^4\Delta$ states, respectively. Taking into account the fact that the bonding situation is similar in these systems it is not a surprise that their dissociation energies differ by less than 4 kcal mol^{-1}.

CuC_2 has a $^2\Sigma$ electronic state which correlates with $4s^13d^{10}+C_2(^1\Sigma_g{}^+)$. The unpaired electron is located in the nonbonding 4s–$3d_{z^2}$ hybrid orbital. Now the metal has 4 π electrons which enter into the M–C_2 π* antibonding orbitals. We therefore find in this compound the shortest C–C distance of the first-row transition-metal dicarbides. The dissociation energy decreases, as expected. For ZnC_2 the extra electron adds again to the nonbonding 4s–$3d_{z^2}$ hybrid orbital.

We now turn to the C_{2v}-symmetric species. Cyclic ScC_2 has a $^2A_1$ state with $4s^23da_1{}^1$ occupation. Two atomic d orbitals belong to the a_1 representation of the C_{2v}-symmetric isomer, namely $3d_{z^2}$ and $3d_{x2-y2}$. The molecular orbitals of this molecule show that the $3d_{z^2}$ orbital mixes with both the 4s orbital and the HOMO of the C_2 fragment increasing the density in the bonding region. The metal $3d_{x2-y2}$ orbital, on the other hand, does not play a major role in the bonding. Instead, it is the main contributor to the $10a_1$ MO which contains the unpaired electron.

For TiC_2 ($^3B_2$) the extra electron adds to the $3db_2$ ($3d_{yz}$) orbital, and for VC_2 ($^4B_1$) to the (nonbonding) $3da_2$ ($3d_{xy}$) orbital. In the titanium and vanadium linear isomers both electrons add to the two nonbonding 3dδ orbitals. Now for the cyclic isomer, $3db_2$ ($3d_{yz}$) mixes with the in-plane antibonding π* orbital of the C_2 fragment.

As commented above, CrC_2 ($^5A_1$) correlates with two asymptotes: $4s^13d^5$ ($3da_1{}^13da_1{}^13db_1{}^13db_2{}^13da_2{}^1$)+$C_2$ ($^3A_1$) and $4s^23d^4$ ($3da_1{}^13db_1{}^13db_2{}^13da_2{}^1$)+$C_2$ ($^1A_1$). Under C_{2v} symmetry, both fragment excitations, namely $^3A_1\leftarrow{}^1A_1$ (C_2) and $4s^23d^4\leftarrow4s^13d^5$ (Cr), involve orbitals belonging to the same representation: a_1. As a consequence, we do not observe an increase in the C–C bond distance and a decrease in its stretching frequency associated with the $^3A_1$ state of C_2, as we have seen in the linear isomer. Moreover, almost no net spin polarization is observed for this isomer. In any case, the dissociation energy of CrC_2 is again about 20 kcal mol^{-1} [CCSD(T) level] less than that of VC_2. With respect to the electronic structure of VC_2 ($^4B_1$), for CrC_2 ($^5A_1$) the extra electron enters into the antibonding combination ($3d_{xz}$–π)*, which partially explains the decrease in the dissociation energy.

In MnC_2 the five 3d orbitals are singly occupied leading to $^6A_1$, as expected. For FeC_2 ($^5A_2$) the extra electron adds to the nonbonding $3da_2$ ($3d_{xy}$) orbital. If the electron enters into one of the two singly occupied $3da_1$ orbitals ($3d_{z^2}$ or $3d_{x^2-y^2}$), equivalent to ScC_2 ($^2A_1$), the state would be $^5A_1$ which lies only 1.6 kcal mol^{-1} above the $^5A_2$ state. For CoC_2 ($^4B_1$) the extra electron adds to the $3db_2$ ($3d_{yz}$) orbital (as in TiC_2 $^3B_2$). Note that the $3db_2$ orbital is now doubly occupied, a fact that should at least partially explain the cyclic topology of this isomer. For NiC_2 ($^3B_1$), the extra electron adds to the $3da_1$ orbital (because the $3da_2$ orbital is already doubly occupied).

The extra electron in CuC_2 ($^2A_1$) enters into the antibonding ($3d_{xz}$–π)* orbital, which is now doubly occupied. The $11a_1$ orbital, which is still singly occupied in CuC_2, is finally filled in ZnC_2 ($^1A_1$). It is clear that for ZnC_2, with the d orbitals fully occupied, M$\leftarrow C_2$ back-donation is not feasible. Furthermore, M$\rightarrow$next-LUMO(C_2) donation should be rather limited because there is a large energy gap between the two sets of orbitals (see Figure 4). The bonding in this

system is therefore mainly due to M→LUMO(C_2) donation. Since zinc has the lowest-lying 4s orbital of all first-row transition metals, the bonding energy is the lowest.

In addition, the results from an energy decomposition analysis (EDA)[52–56] of MC_2 compounds are shown in Table 7 (Sc–Mn) and Table 8 (Fe–Zn). Within this formalism the total interaction energy is partitioned into different components: 1) ΔE_{elstat} is the electrostatic interaction energy between the fragments, calculated with a frozen electron distribution in the geometry of the compound, 2) ΔE_{pauli} is the repulsive term arising from exchange repulsion, and 3) ΔE_{orb} is the stabilization due to orbital interactions, a term which can be separated into the interactions arising from the different symmetries within the point group of the molecule. The sum of these three terms gives the total interaction energy, ΔE_{int}. Finally, in order to obtain the total bond energy, one must take into account the preparation energy, ΔE_{prep}, that is, the energy necessary to promote both fragments (M and C_2 in our case) from their equilibrium geometry and electronic ground state to the geometry and electronic state of the MC_2 molecule. Further information and technical details about this method can be found in refs. [52] and [53]. The EDA analysis was carried out with the BP86 functional[57,58] employing a STO triple-zeta basis set augmented by one set of d and f polarization functions on carbon and one set of p- (diffuse) and f-type (polarization) functions on the metal.[59] The $1s^2$ core electrons of the carbon atoms and the $1s^22s^22p^6$ core electrons of the metal atom were treated by the frozen core approximation.[60] The EDA analysis was carried out using geometries optimized at

Table 7. Energy decomposition analysis [kcal mol^{-1}] of M–C_2 (M = Sc, Ti, V, Cr, Mn) at the BP86/TZ2P+ level of theory.

		Sc		Ti		V		Cr		Mn	
C_{2v}	ΔE_{int}	−165.6		−167.5		−173.9		−108.0		−130.1	
	ΔE_{pauli}	260.1		339.4		393.0		197.7		308.1	
	ΔE_{elstat}	−160.9	(37.8%)[a]	−207.4	(40.9%)	−238.2	(42.0%)	−113.0	(37.0%)	−190.2	(43.4%)
	ΔE_{orb}	−264.8	(62.2%)	−299.4	(59.1%)	−328.7	(58.0%)	−192.8	(63.0%)	−248.0	(56.6%)
	$\Delta E(a_1)$	−229.3	(86.6%)[b]	−237.1	(79.2%)	−258.2	(78.6%)	−153.7	(79.8%)	−209.8	(84.6%)
	$\Delta E(a_2)$	0.0	(0.0%)	0.0	(0.0%)	−3.3	(1.0%)	−2.1	(1.1%)	−0.7	(0.3%)
	$\Delta E(b_1)$	−15.1	(5.7%)	−22.7	(7.6%)	−27.7	(8.4%)	−10.4	(5.4%)	−13.1	(5.3%)
	$\Delta E(b_2)$	−20.5	(7.7%)	−39.7	(13.2%)	−39.4	(12.0%)	−26.5	(13.8%)	−24.4	(9.8%)
$C_{\infty v}$	ΔE_{int}	−150.3		−152.6		−159.2		−97.6		−124.8	
	ΔE_{pauli}	181.1		189.5		188.3		176.3		187.9	
	ΔE_{elstat}	−89.2	(26.9%)	−86.0	(25.1%)	−79.8	(23.0%)	−115.1	(42.0%)	−84.2	(26.9%)
	ΔE_{orb}	−242.2	(73.1%)	−256.1	(74.9%)	−267.7	(77.0%)	−158.9	(58.0%)	−228.5	(73.1%)
	$\Delta E(\sigma)$	−201.6	(83.2%)	−205.8	(80.4%)	−209.4	(78.2%)	−93.3	(58.7%)	−187.4	(82.0%)
	$\Delta E(\pi)$	−40.6	(16.8%)	−50.6	(19.7%)	−59.2	(22.1%)	−64.5	(40.6%)	−41.4	(18.1%)
	$\Delta E(\delta)$	0.0	(0.0%)	0.2	(0.0%)	+0.9	(-0.3%)	−1.0	(0.6%)	0.2	(0.0%)

[a] Values in parentheses give the percentage of attractive interactions $\Delta E_{elstat} + \Delta E_{orb}$. [b] Values in parentheses give the percentage contribution to the total orbital interactions.

Table 8. Energy decomposition analysis [kcal mol^{-1}] of M–C_2 (M = Fe, Co, Ni, Cu, Zn) at the BP86/TZ2P+ level of theory.

		Fe		Co		Ni		Cu		Zn	
C_{2v}	ΔE_{int}	−143.0		−153.8		−186.4		−112.1		−69.9	
	ΔE_{pauli}	347.0		406.2		397.6		232.5		249.0	
	ΔE_{elstat}	−212.4	(43.4%)[a]	−248.7	(44.4%)	−243.4	(41.7%)	−162.1	(47.0%)	−150.2	(47.1%)
	ΔE_{orb}	−277.5	(56.6%)	−311.2	(55.6%)	−340.7	(58.3%)	−182.5	(53.0%)	−168.6	(52.9%)
	$\Delta E(a_1)$	−227.4	(81.9%)[b]	−241.9	(77.7%)	−269.9	(79.2%)	−152.9	(83.8%)	−148.3	(87.9%)
	$\Delta E(a_2)$	−4.8	(1.7%)	−4.7	(1.5%)	−4.3	(1.3%)	−1.1	(0.6%)	−0.1	(0.1%)
	$\Delta E(b_1)$	−16.7	(6.0%)	−23.9	(7.7%)	−30.4	(8.9%)	−5.1	(2.8%)	−6.8	(4.0%)
	$\Delta E(b_2)$	−28.7	(10.3%)	−40.8	(13.1%)	−36.0	(10.6%)	−23.4	(12.8%)	−13.4	(8.0%)
$C_{\infty v}$	ΔE_{int}	−133.9		−133.4		−147.1		−102.4		−68.7	
	ΔE_{pauli}	202.1		221.1		218.8		130.3		140.3	
	ΔE_{elstat}	−86.1	(25.6%)	−104.3	(29.4%)	−99.1	(27.1%)	−75.4	(32.4%)	−68.8	(32.9%)
	ΔE_{orb}	−249.9	(74.4%)	−250.3	(70.6%)	−266.9	(72.9%)	−157.3	(67.6%)	−140.2	(67.1%)
	$\Delta E(\sigma)$	−199.0	(79.6%)	−189.1	(75.6%)	−193.0	(72.3%)	−143.3	(91.1%)	−123.5	(88.1%)
	$\Delta E(\pi)$	−51.2	(20.5%)	−61.1	(24.4%)	−74.3	(27.8%)	−14.4	(9.1%)	−16.9	(12.1%)
	$\Delta E(\delta)$	0.3	(0.0%)	−0.1	(0.0%)	+0.4	(0.0%)	−0.3	(0.0%)	0.2	(0.0%)

[a] Values in parentheses give the percentage of attractive interactions $\Delta E_{elstat} + \Delta E_{orb}$. [b] Values in parentheses give the percentage contribution to the total orbital interactions.

the same level of theory. Only the relevant data from the EDA analysis are shown in Table 7 and Table 8.

We would like to stress that the EDA results should not be overinterpreted because they have been computed at the BP86 level of theory. We have seen already that the energies and geometrical parameters computed at the B3LYP level of theory differ in some cases from the coupled-cluster ones. As expected, the BP86 results are not much better. For this reason we will not report the dissociation energies obtained at this level of theory in Table 7 and Table 8. In any case we think that we can extract some important information from the partitioning of the BP86 interaction energies.

We will begin by commenting on the most interesting results obtained for the linear isomers. The EDA results show that more than $^2/_3$ of the stabilizing contributions come from the orbital term. This makes sense because atoms have no electrostatic multipole moment. The exception is CrC_2, for which the electrostatic contribution increases to 42% as a result of the small orbital term (we will come back to this point later). The orbital term splits into σ and π contributions. The data collected in Table 7 and Table 8 show that 72–83% of the orbital attraction comes from the σ contribution (note that the transfer of almost one electron from the metal atom to the C_2 unit, as suggested by the NBO charges, takes place mostly in this representation). The exceptions are CrC_2 for which the σ term drops to 58.7% and CuC_2 and ZnC_2 for which it increases to 91.1 and 88.1%, respectively. The decrease observed for CrC_2 should be related to the spin polarization of the α and β densities as commented above. Note that the Pauli repulsion in CrC_2 is similar to that found in the other systems and that the electrostatic attraction even increases slightly. Thus, CrC_2 has a lower dissociation energy because of its weaker σ bond. CuC_2 and ZnC_2 have very little π stabilization because the four 3dπ electrons enter into antibonding orbitals. Finally, the EDA results show that the 3dδ electrons produce negligible stabilization in the linear systems.

In the cyclic isomers the orbital term accounts for 52.9–63% of the total attractive interactions. This contribution is thus smaller (as a percentage) than the one found in the linear species. Note that the orbital term itself is actually slightly larger for the C_{2v}-symmetric isomers (as a result of greater overlapping between the corresponding orbitals, as commented on before). The reason why its relative contribution is smaller is the striking increase in the electrostatic contribution (between 90–180%). The larger contribution of the electrostatic forces in the cyclic isomers should be related to the fact that the C_2 fragment in its $^1\Sigma_g^+$ state has a more diffuse charge-density distribution in the region perpendicular to the molecular axes than along the axes. [We would like to remind the reader that the electrostatic attraction between the fragments is not due to the interaction between (permanent) multipole moments because the metal atom lacks them, but rather to the overlap of the charge densities.] However, this stronger electrostatic attraction in the C_{2v}-symmetric species does not explain by itself the conformational preference, for the repulsive ΔE_{pauli} term also increases in these isomers (between 55–109%). Note that if we sum up ΔE_{pauli} and ΔE_{elstat} we get larger positive numbers for the cyclic species, that is, consideration of these two terms alone would favor the linear isomers. To obtain the correct preference for the C_{2v}-symmetric species it is necessary to take into account again the orbital contributions. We see then that the conformational preference must be explained in terms of more favorable stabilizing contributions (electrostatic and orbital) for the cyclic isomers which are not counterbalanced by the larger Pauli repulsion energy in these species.[61] Moreover, the EDA results clearly show that, among the stabilizing interactions, the electrostatic forces contribute most to the conformational preference. In this sense, we could conclude that the cyclic isomers of the transition-metal dicarbides are favored over the linear ones because of the much more favorable electrostatic interactions in the former.

Finally, we can compare our results for the first-row transition-metal dicarbides with the stability of met-cars. Based on theoretical[62–65] and experimental[66,67] work, it is generally assumed that the preferred structure of M_8C_{12} met-cars is a tetracapped tetrahedron with T_d symmetry.[6] In this structure there are two types of metal atoms: 1) the atoms that are bonded side-on (π-bonded) to three dicarbon moieties and 2) the atoms that are bonded end-on (σ-bonded) also to three dicarbon moieties. Therefore, it seems that the basic structural subunit should be MC_2. This view can be confirmed by comparison of the bonding energies (per atom) of the first-row met-cars with the dissociation energies of the corresponding dicarbides. These two parameters, computed by employing DFT, are shown in Figure 5. The bonding energies for the T_d met-cars are taken from the work of Rohmer et al.[6] As can be seen in Figure 5, there is a clear correlation between both parameters. Of course, there are important discrepancies, such as the opposite relative stability of the scandium and titanium compounds or the large drop for CrC_2. Met-cars are much more complex than dicarbides and therefore there should be other factors that influ-

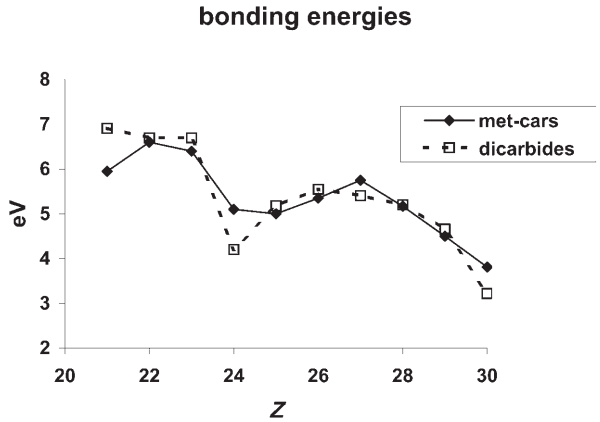

Figure 5. Comparison of the dissociation energies for the first-row transition-metal dicarbides with the bonding energies (per atom) for the corresponding met-cars (taken from ref. [6]) computed at the DFT level of theory. All values are given in eV.

ence their relative stability. Nevertheless, even with these limitations in mind, we think that the results shown in Figure 5 clearly illustrate that the global trends observed for the relative stability of met-cars with different transition metals are very similar to those observed for the corresponding dicarbides. The evolution from scandium to copper is very similar for both parameters, showing that early transition metals have a greater tendency to form met-cars than late transition metals. This seems to be mainly due, according to the trends observed in Figure 5, to the higher stability of the early transition-metal dicarbides.

Conclusion

The molecular structures of the first-row transition-metal dicarbides MC_2 (M = Sc–Zn) have been studied theoretically. Special attention has been paid to the competition between linear and cyclic isomers. In agreement with previous studies it has been found that all the systems preferred a C_{2v}-symmetric arrangement. Topological analysis of the electron density has revealed that for TiC_2, CoC_2, and NiC_2, the C_{2v}-symmetric isomer corresponds to a true ring structure with peripheral X–C bonds. On the other hand, for the rest of the dicarbides the C_{2v}-symmetric isomer corresponds in fact to a T-shaped structure.

A detailed analysis of the variation of the energy of the dicarbides with the angle between the metal atom and the midpoint of the C–C bond has been carried out. This study has provided a deeper understanding of the factors governing the linear–cyclic competition of these compounds. It was found that the energy difference between the linear and C_{2v}-symmetric species in general decreases when moving towards the right side of the transition series. Therefore, early transition metals have a greater tendency to coordinate to both carbon atoms than late transition metals. Furthermore, in general, early transition metals have larger dissociation energies than late transition metals. These characteristics might be related to a preference to form different materials when first-row transition metals interact with carbon. In fact, it has been shown that there is a good correlation between the dissociation energies of first-row transition-metal dicarbides and the bonding energies observed for the corresponding met-cars.

The main features of these compounds have been rationalized in terms of the most relevant interactions between the valence orbitals of the metal atom and the C_2 fragment. It is hoped that this study could help in understanding the behavior of other transition-metal carbon clusters.

Acknowledgements

This research was supported by the Ministerio de Ciencia y Tecnología of Spain (Grant CTQ2004-07405-C02-01) and by the Junta de Castilla y León (Grant VA 085/03). We thank Dr. I. S. K. Kerkines (National and Kapodistrian University of Athens) for helpful comments regarding the multiconfigurational calculations.

[1] B. C. Guo, K. P. Kearns, A. W. Castleman, *Science* **1992**, *255*, 1411–1413.
[2] B. C. Guo, S. Wei, J. Purnell, S. Buzza, A. W. Castleman, *Science* **1992**, *256*, 515–516.
[3] S. Wei, B. C. Guo, J. Purnell, S. Buzza, A. W. Castleman, *Science* **1992**, *256*, 818–820.
[4] S. Wei, B. C. Guo, J. Purnell, S. Buzza, A. W. Castleman, *J. Phys. Chem.* **1992**, *96*, 4166–4168.
[5] J. S. Pilgrim, M. A. Duncan, *J. Am. Chem. Soc.* **1993**, *115*, 6958–6961.
[6] M. M. Rohmer, M. Benard, J. M. Poblet, *Chem. Rev.* **2000**, *100*, 495–542.
[7] S. Iijima, T. Ichihashi, *Nature*, **1993**, *363*, 603–605.
[8] D. E. Clemmer, J. M. Hunter, K. B. Shelomov, M. E. Jarrold, *Nature* **1994**, *372*, 248–250.
[9] Y. Chai, T. Guo, C. Jin, R. E. Haufler, L. P. F. Chibante, J. Fure, L. Wang, J. M. Alford, R. E. Smalley, *J. Phys. Chem.* **1991**, *95*, 7564–7568.
[10] A. Largo, P. Redondo, C. Barrientos, *J. Am. Chem. Soc.* **2004**, *126*, 14611–14619.
[11] B. K. Nash, B. K. Rao, P. Jena, *J. Chem. Phys.* **1996**, *105*, 11020–11023.
[12] Z. Cao, *J. Mol. Struct. (Theochem)* **1996**, *365*, 211–214.
[13] S. Roszak, K. Balasubramanian, *J. Phys. Chem. A* **1997**, *101*, 2666–2669.
[14] R. Sumathi, M. Hendrickx, *Chem. Phys. Lett.* **1998**, *287*, 496–502.
[15] P. Jackson, G. E. Gadd, D. W. Mackey, H. van der Wall, G. D. Willett, *J. Phys. Chem. A* **1998**, *102*, 8941–8945.
[16] A. V. Arbuznikov, M. Hendrickx, L. G. Vanquickenborne, *Chem. Phys. Lett.* **1999**, *310*, 515–522.
[17] A. V. Arbuznikov, M. Hendrickx, *Chem. Phys. Lett.* **2000**, *320*, 575–581.
[18] C. Rey, M. M. G. Alemany, O. Dieguez, L. J. Gallego, *Phys. Rev. B* **2000**, *62*, 12640–12643.
[19] E. G. Noya, R. C. Longo, L. J. Gallego, *J. Chem. Phys.* **2003**, *119*, 11130–11134.
[20] D. Majumdar, S. Roszak, K. Balasubramanian, *J. Chem. Phys.* **2003**, *118*, 130–141.
[21] H. J. Zhai, L. S. Wang, P. Jena, G. L. Gutsev, C. W. Bauschlicher Jr., *J. Chem. Phys.* **2004**, *120*, 8996–9008.
[22] M. F. A. Hendrickx, S. Clima, *Chem. Phys. Lett.* **2004**, *388*, 284–289.
[23] M. F. A. Hendrickx, S. Clima, *Chem. Phys. Lett.* **2004**, *388*, 290–296.
[24] M. V. Ryzhkov, A. L. Ivanovskii, B. T. Delley, *Chem. Phys. Lett.* **2005**, *404*, 400–408.
[25] R. Haque, K. A. Gingerich, *J. Chem. Phys.* **1981**, *74*, 6407–6414.
[26] X. B. Wang, C. F. Ding, L. S. Wang, *J. Phys. Chem. A* **1997**, *101*, 7699–7701.
[27] X. Li, L. S. Wang, *J. Chem. Phys.* **1999**, *111*, 8389–8395.
[28] A. D. Becke, *J. Chem. Phys.* **1986**, *84*, 4524–4529.
[29] A. D. Becke, *J. Chem. Phys.* **1988**, *88*, 2547–2553.
[30] G. Pascoli, H. Lavendy, *Int. J. Mass Spectrom.* **1998**, *181*, 11–25.
[31] C. Lee, W. Yang, R. G. Parr, *Phys. Rev. B* **1988**, *37*, 785–789.
[32] A. D. Becke, *J. Chem. Phys.* **1988**, *88*, 1053–1062.
[33] J. A. Pople, M. Head-Gordon, K. Raghavachari, *J. Chem. Phys.* **1987**, *87*, 5968–5975.
[34] R. Krishnan, J. S. Binkley, R. Seeger, J. A. Pople, *J. Chem. Phys.* **1980**, *72*, 650–654.
[35] A. J. H. Wachters, *J. Chem. Phys.* **1970**, *52*, 1033–1036.
[36] P. J. Hay, *J. Chem. Phys.* **1977**, *66*, 4377–4384.
[37] K. Raghavachari, G. W. Trucks, *J. Chem. Phys.* **1989**, *91*, 1062–1065.
[38] K. Raghavachari, G. W. Trucks, J. A. Pople, M. Head-Gordon, *Chem. Phys. Lett.* **1989**, *157*, 479–483.
[39] Gaussian 98 (Revision A.7), M. J. Frisch, G. W. Trucks, H. B. Schlegel, G. E. Scuseria, M. A. Robb, J. R. Cheeseman, V. G. Zakrzewski, J. A. Montgomery, R. E. Stratmann, J. C. Burant, S. Dapprich, J. M. Millam, A. D. Daniels, K. N. Kudin, M. C. Strain, O. Farkas, J. Tomasi, V. Barone, M. Cossi, R. Cammi, B. Mennucci, C. Pomelli, C. Adamo, S. Clifford, J. Ochterski, G. A. Petersson, P. Y. Ayala, Q.

Cui, K. Morokuma, D. K. Malick, A. D. Rabuck, K. Raghavachari, J. B. Foresman, J. Cioslowski, J. V. Ortiz, A. G. Baboul, B. B. Stefanov, G. Liu, A. Liashenko, P. Piskorz, I. Komaromi, R. Gomperts, R. L. Martin, D. J. Fox, T. Keith, M. A. Al-Laham, C. Y. Peng, A. Nanayakkara, C. Gonzalez, M. Challacombe, P. M. W. Gill, B. G. Johnson, W. Chen, M. W. Wong, J. L. Andres, M. Head-Gordon, E. S. Replogle, J. A. Pople, Gaussian, Inc., Pittsburgh, PA, **1998**.

[40] K. Pierloot in *Computational Organometallic Chemistry* (Ed.:T. R. Cundari), Marcel Decker, Inc., New York, **2001**, p. 125.

[41] K. Andersoon, B. O. Roos, *Chem. Phys. Lett.* **1992**, *191*, 507–514.

[42] MOLPRO, a package of ab initio programs designed by H.-J. Werner and P. J. Knowles, version 2002.1, R. D. Amos, A. Bernhardsson, A. Berning, P. Celani, D. L. Cooper, M. J. O. Deegan, A. J. Dobbyn, F. Eckert, C. Hampel, G. Hetzer, P. J. Knowles, T. Korona, R. Lindh, A. W. Lloyd, S. J. McNicholas, F. R. Manby, W. Meyer, M. E. Mura, A. Nicklass, P. Palmieri, R. Pitzer, G. Rauhut, M. Schütz, U. Schumann, H. Stoll, A. J. Stone, R. Tarroni, T. Thorsteinsson, H.-J. Werner, **2002**.

[43] R. W. F. Bader, *Atoms in Molecules. A Quantum Theory*, Clarendon Press, Oxford, **1990**.

[44] P. L. A. Popelier, *Comput. Phys. Commun.* **1996**, *93*, 212–240.

[45] A. E. Reed, L. A. Curtiss, F. Weinhold, *Chem. Rev.* **1988**, *88*, 899–926.

[46] R. F. W. Bader, *Chem. Rev.* **1991**, *91*, 893–928.

[47] D. Cremer, E. Kraka, *Angew. Chem.* **1984**, *96*, 612–614; *Angew. Chem. Int. Ed. Engl.* **1984**, *23*, 627–628.

[48] G. Frenking, N. Frohlich, *Chem. Rev.* **2000**, *100*, 717–774.

[49] E. Clementi, H. Kistenmacher, H. Popkie, *J. Chem. Phys.* **1973**, *58*, 2460–2466.

[50] M. L. Abrams, C. D. Sherrill, *J. Chem. Phys.* **2004**, *121*, 9211–9219.

[51] C. D. Sherrill, P. Piecuch, *J. Chem. Phys.* **2005**, *122*, 124104.

[52] K. Morokuma, *J. Chem. Phys.* **1971**, *55*, 1236–1244.

[53] K. Morokuma, *Acc. Chem. Res.* **1977**, *10*, 294–300.

[54] T. Ziegler, A. Rauk, *Theor. Chim. Acta* **1977**, *46*, 1–10.

[55] F. M. Bickelhaupt, E. J. Baerends, *Rev. Comput. Chem.* **2000**, *15*, 1–86.

[56] G. te Velve, F. M. Bickelhaupt, E. J. Baerends, S. J. A. van Gisbergen, C. Fonseca Guerra, J. G. Snijders, T. Ziegler, *J. Comput. Chem.* **2001**, *22*, 931–967.

[57] A. D. Becke, *Phys. Rev. A* **1988**, *38*, 3098–3100.

[58] J. P. Perdew, *Phys. Rev. B* **1986**, *33*, 8822–8824.

[59] J. G. Snijders, E. J. Baerends, P. Vernooijs, *At. Nucl. Data Tables* **1982**, *26*, 483–509.

[60] E. J. Baerends, D. E. Ellis, P. Ros, *Chem. Phys.* **1973**, *2*, 41–51.

[61] This is not a trivial result as a stronger bond may come from less Pauli repulsion. See, for example: a) C. Esterhuysen, G. Frenking, *Theor. Chem. Acc.* **2004**, *111*, 381–389; b) F. M. Bickelhaupt, R. L. DeKock, E. J. Baerends, *J. Am. Chem. Soc.* **2002**, *124*, 1500–1505.

[62] I. J. Dance, *J. Am. Chem. Soc.* **1996**, *118*, 2699–2707.

[63] I. J. Dance, *J. Am. Chem. Soc.* **1996**, *118*, 6309–6310.

[64] J. M. Poblet, M. M. Rohmer, M. Benard, *Inorg. Chem.* **1996**, *35*, 4073–4075.

[65] H. Hou, J. T. Muckerman, P. Liu, J. A. Rodriguez, *J. Phys. Chem. A* **2003**, *107*, 9344–9356.

[66] L. S. Wang, S. Li, H. Wu, *J. Phys. Chem.* **1996**, *100*, 19211–19214.

[67] S. Li, H. Wu, L. S. Wang, *J. Am. Chem. Soc.* **1997**, *119*, 7417–7422.

Received: March 8, 2006
Published online: June 14, 2006

